FLOW STRUCTURE FROM A HORIZONTAL CYLINDER COINCIDENT WITH A FREE SURFACE IN SHALLOW WATER FLOW

by

***Ali KAHRAMAN*[a*]*, Muammer ÖZGÖREN*[b]*, Beşir ŞAHİN*[c]**

[a]Mechanical Education Department, Selçuk University, Konya, Turkey
[b]Department of Mechanical Engineering, Selçuk University, Konya, Turkey
[c]Department of Mechanical Engineering, Çukurova University, Adana, Turkey

Vortex formation from a horizontal cylinder coincident with a free surface of a shallow water flow having a depth of 25.4 [mm] was experimentally investigated using the PIV technique. Instantaneous and time-averaged flow patterns in the wake region of the cylinder were examined for three different cylinder diameter values under the fully developed turbulent boundary layer condition. Reynolds numbers were in the range of $1124 \leq Re \leq 3374$ and Froude numbers were in the range of $0.41 \leq Fr \leq 0.71$ based on the cylinder diameter. It was found that a jet-like flow giving rise to increasing the flow entrainment between the core and wake regions depending on the cylinder diameter was formed between the lower surface of the cylinder and bottom surface of the channel. Vorticity intensity, Reynolds stress correlations and the primary recirculating bubble lengths were grown to higher values with increasing the cylinder diameter. On the other hand, in the case of the lowest level of the jet-like flow emanating from the beneath of the smallest cylinder, the variation of flow characteristics were attenuated significantly in a shorter distance. The variation of the reattachment location of the separated flow to the free-surface is a strong function of the cylinder diameter and the Froude number.

Key words: *horizontal cylinder, PIV, reattachment, shallow water flow, vorticity, wake region*

1. Introduction

The shallow water flow is defined as the situation where the horizontal length scale of a typical eddy is significantly larger than the vertical extent of the flow, which means that the dominating processes take place in the horizontal plane [1, 2]. Free-shear flows from the cylinder lead to vortex generation in shallow water, whereby the characteristic diameter of the vortex is larger than the water depth. This class of vortices occurs in a wide variety of hydraulic, environmental and geophysical flow applications such as large obstacles, islands, stranded oil tankers, pipe lines, offshore structures, marines and large-scale bridge piers [3].

Studies of Ingram and Chu [4], Chen and Jirka [5], Akilli and Rockwell [2], Kahraman et al. [1], Akilli et al. [6] show that the flow structure downstream behind bluff bodies in shallow water is different comparing to the deep water flow in the cases of vertical cylinder applications. Ingram and Chu [4] considered both full-scale and scaled models of bluff body wakes and addressed the roles of transverse shear and bed friction effects. Chen and Jirka [5] experimentally characterized shallow wakes of bluff bodies and defined three basic classes of wake patterns. Akilli and Rockwell [2] characterized the structure of vortex formation in the near wake of a cylinder as a function of elevation above the bed in terms of vorticity and streamline patterns. Although the flow structure around the vertical cylinder has been generally investigated, very little attention has been given to the behavior of flow past the horizontal cylinder placed close to the free-surface. It is worth noting that the limited water depth in shallow water flow prevents the development of three-dimensional instabilities. In addition to the water depth, the bottom friction which acts as a mechanism for suppression of the transverse growth of disturbance plays an important role in the development of the turbulent wake in shallow water flow.

Flow past a bluff body which is placed in a horizontal plane and normal to the free stream, close or piercing to the free surface in deep water flow has been investigated experimentally and theoretically. The stability of the flow past a half-submerged cylinder as a function of Froude number was examined by Triantafyllou and Dimas [7, 8]. For the limiting case of a cylinder piercing a free surface, they demonstrated analytically that the near wake could exhibit a convective, as opposed to a global (or absolute), instability. Yu and Tryggvason [9] investigated the free-surface signature of unsteady two-dimensional vortex flows numerically. Their major finding was that the dominant parameter governing surface deformation was the Froude number. Tryggvason et al. [10] addressed that surface tension acted to limit strong surface curvature, thereby reducing the production of secondary vorticity at the surface. This can significantly modify the interaction of vortices with a free surface at high Froude numbers if the surface tension is significant. A detailed discussion of the vorticity and free surfaces, including many illuminating examples, was given by Rood [11]. The flow behavior of a cylinder near a free-surface for Fr=0.60 and h/d =0.45 was considered by Sheridan et al. [12]. For this parameter set, two admissible wake states were observed. Each state was found to possess limited stability such that transformations from one state to the other occurred in a time-dependent manner. Thus, the flow was categorized as metastable. In the other study of Sheridan et al. [13], a region of parameter space for the cylinder close to the free water surface was investigated with a wide variety of different wake behaviors. They concluded that the jet of fluid passing over the cylinder exhibited a number of possible states including: attachment to the free surface; attachment to the cylinder; and an intermediate state in between. They also stated that flow past a cylinder in an unbounded medium gives rise to self-sustained, limit cycle oscillations involving formation of large-scale Kármán vortices. Hoyt and Sellin [14] confirmed some of the findings of Sheridan et al. [13] and provided some further details on the time-dependence. On the other hand, when the cylinder was located sufficiently close to a solid wall, Bearman and Zdravkovich [15] demonstrated cessation of the Karman formation. Reichl et al. [16] presented some results from computations of the flow at Re=180, mainly focusing on the evolution of the vorticity field for the metastable state that was first described by Sheridan et al. [12]. Recently, flow past a cylinder placed close to a free-surface has been numerically investigated by Reichl et al. [17] having Reynolds number and Froude number as Re=180 and 0.0<Fr<0.7, respectively. They concentrated on the main effects of gap ratio and Froude number together with details of the variation of physical parameters. They obtained particularly good agreement with the experimental results of Sheridan et al. [12, 13] for their larger Froude number.

Recently, Ozturk et al. [18] and Sahin and Ozturk [19] have investigated the flow characteristics in the wake region of a vertical cylinder at the junction of cylinder and base plate in the fully developed boundary layer.

The unsteady structure of the flow downstream of the horizontal cylinder in close proximity has not been investigated in detail in the case of the shallow water flows. The present investigation is to characterize the possible wake structures when the cylinders having different diameters are located in the immediate vicinity of the free surface, without piercing it. In this sense, the aim of the present work is to obtain quantitative information on the downstream flow characteristics of the horizontal cylinder in the shallow water flow using the particle image velocimetry (PIV) technique. Instantaneous and time-averaged flow patterns are presented both in side-view and end-view planes in order to provide quantitative information and hence interpret the flow structure from the point of flow physics.

2. Experimental System and Techniques

Experiments were performed in a large-scale water channel, having a test section length of 4318 [mm] and width 610 [mm], at Lehigh University in the Fluid Mechanics Laboratory of Department of Mechanical Engineering and Mechanics. The test section was preceded by a large reservoir and a 3:1 contraction. A system of honeycomb and screens were employed immediately upstream of the contraction, in order to obtain a turbulence level in the free-stream below 0.1%. In order to study the case of a shallow water layer, the test section was filled with water to a level of h_w=25.4 [mm] and this water level was maintained constant for all experiments. A schematic view of the cylinder arrangement is shown in the plan-view and side-view planes in fig. 1. Three different cylinder diameters D =19.05 [mm], 12.70 [mm] and 6.35 [mm] were employed. The values of dimensionless diameter with respect to water depth D/h_w were 0.75, 0.50 and 0.25. The maximum velocity of the fully developed turbulent water layer was maintained at 177.8 [mm/s] during all experiments. The corresponding values of Reynolds number based on the cylinder diameter were Re=3373.6, 2249.1 and 1124.6. The Froude number based on the water depth h_w was Fr=$U/(gh_w)^{1/2}$=0.36. The Froude number can also be defined as Fr=$U/(gD)^{1/2}$, which were 0.41, 0.50 and 0.71 according to the aforementioned cylinder diameters.

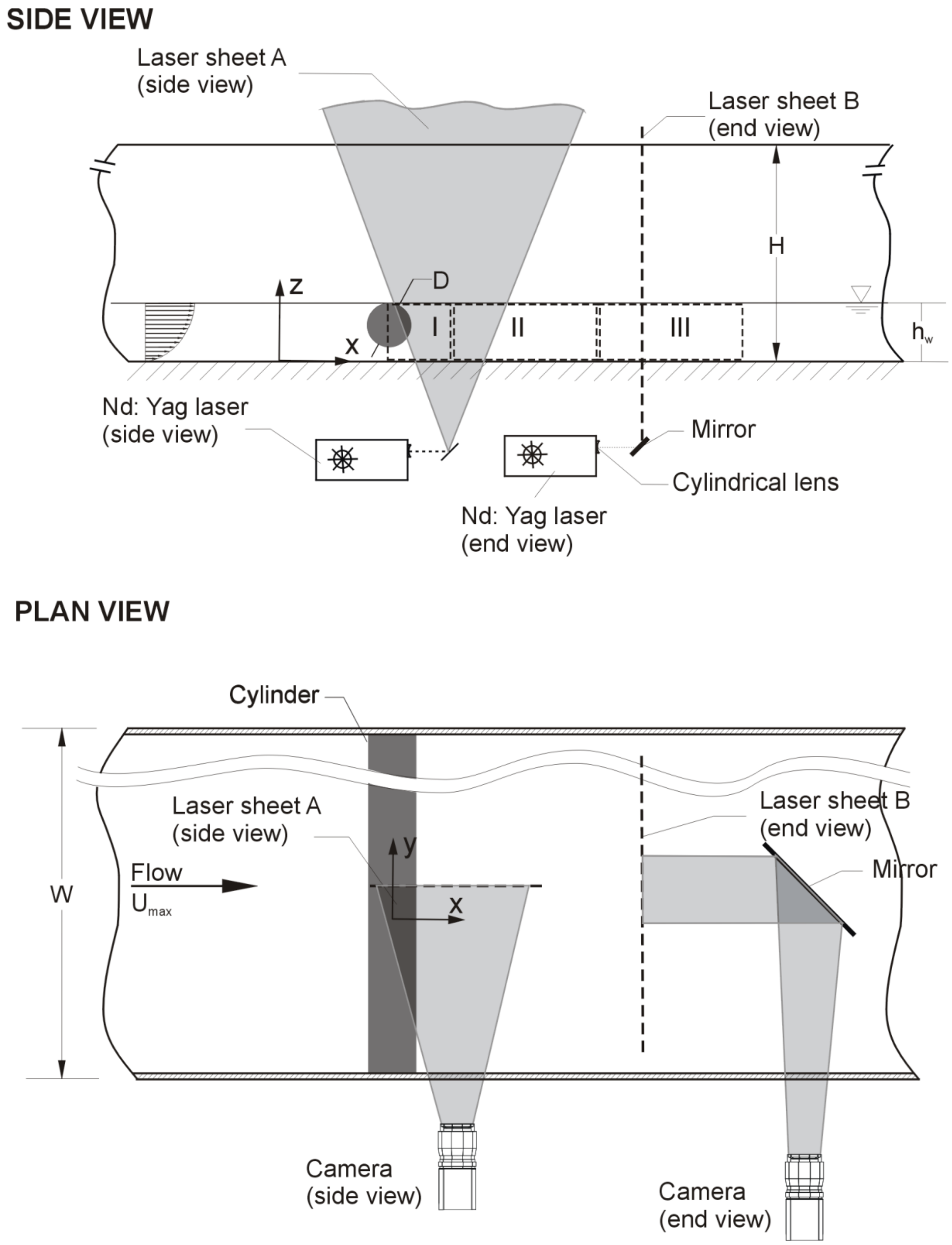

Figure 1. Overview of a horizontal cylinder in shallow water, and deployment of laser sheet

In order to ensure that the shallow layer corresponded to a fully-developed turbulent flow at the streamwise location of interest, as specially-designed boundary layer trip wire was placed in horizontal direction normal to the free stream along the width of the channel bottom at its entrance. It involved a small-diameter (1.57 [mm]) rod wound with wire of 0.90 [mm] for the maximum velocity U_{max} =177.8 [mm/s] of the water layer. In absence of the horizontal cylinder, the time-averaged distribution of the streamwise velocity along the water depth at the horizontal cylinder location is shown in fig. 2. This cylinder was positioned a distance of 2845 [mm] from the leading edge of the test section, in order to allow development of a fully turbulent boundary layer, according to the criteria of Kirkgoz and Ardiclioglu [20]. As seen in fig. 2, the distribution of averaged velocity agreed well with those of Klebanoff [21], Purtel et al. [22], Johansen and Smith [23] and Kirkgoz and Ardiclioglu [20]. Furthermore, the ratios of the displacement δ^* and momentum θ thicknesses relative to the boundary layer thickness (i.e. the water depth h_w) were found to be δ^*/δ = 0.17 and θ/δ= *0.13 respectively*. The boundary layer shape factor $H=\delta^*/\theta$ was 1.31, which was in the well known range of 1.2<H<1.4 for fully developed turbulent flow.

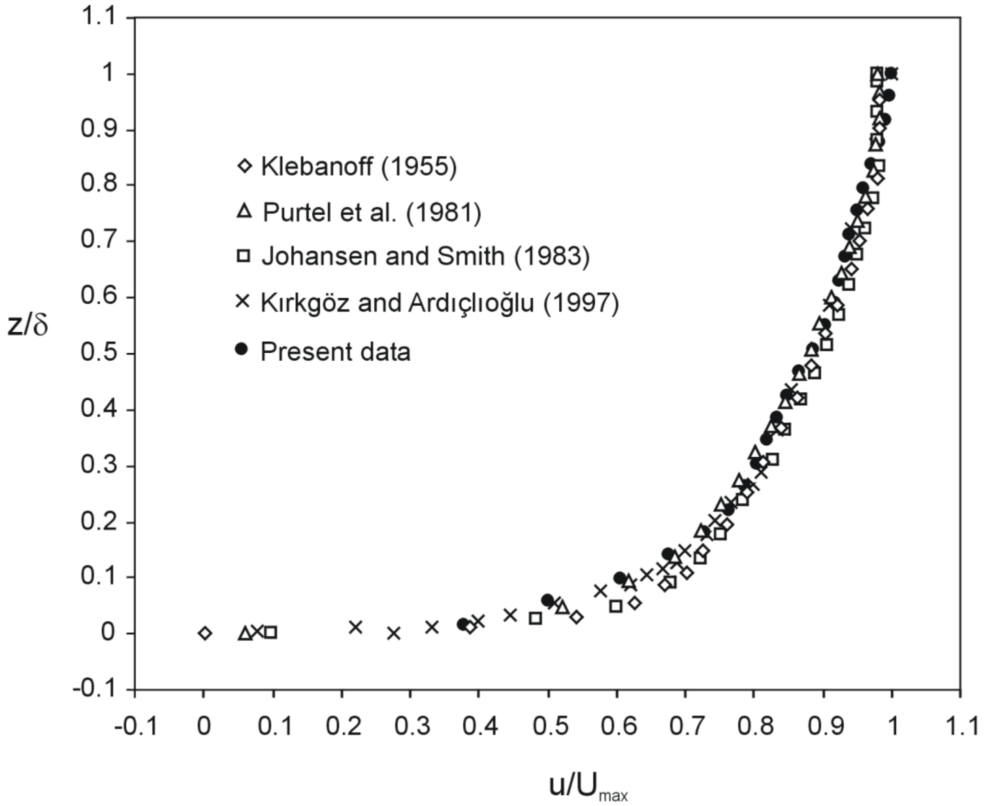

Figure 2. Velocity distributions for fully developed turbulent boundary layer

Use of high-image-density particle image velocimetry (PIV) allowed determination of the instantaneous velocity distribution over the entire plane of interest. Of course, since the flow patterns addressed herein are unsteady, there will be deviations from one instantaneous image to the next image, and therefore these snapshots of the flow field must be interpreted with caution in attempting to deduce the time-averaged state of the flow. In order to characterize the flow structure downstream of the cylinder, the PIV technique was employed. The flow was seeded with 14.6 [μm] metallic coated particles, which were essentially neutrally buoyant. Laser sheets, designated as A and B in fig. 1. were generated using a double-pulsed Nd:Yag laser system (120 [mJ]). Patterns of particle images were acquired by the CCD camera having a resolution of 1000 pixels × 1016 pixels at a rate of 15 [frames/s], with a time delay between frames from 2 [ms] to 3 [ms] with an image capturing frequency of 15 [Hz]. A frame-to-frame cross correlation technique with an interrogation window of 16 pixels × 16 pixels was employed to determine the velocity field. During the interrogation process, an overlap of 50% was employed in order to satisfy the Nyquist criterion. The number of particle images within the interrogation window, accounting for both pulses of the laser, was of the order of 100, which exceeded the criterion high-image-density. The camera was equipped with a 55 [mm] lens. The laser sheet thickness was approximately 1.5 [mm]. The distance from the plane of the laser sheet to the lens of the camera was 508 [mm]. The magnification in the field of view was 1:15.2 for side view images yielding a grid size 1.05 × 1.05 [mm] in physical plane of the laser sheet and total velocity vectors 1525 (61 × 25). On the other hand, the magnification values were changing from 1:12.3 to 1:13.9 for end-view images depending on the laser sheet location, which provided total velocity vectors 800 (40 × 20) and grid sizes in the range of 1.15 × 1.15 [mm] to 1.30 × 1.30 [mm]. During the course of the experiment, images were separately acquired over different fields of side-view as indicated in the schematic of fig. 1. This approach was necessary in order to attain sufficient spatial resolution. Images acquired in each of these fields of view were averaged, and by splicing them together, it is possible to define this flow structure over a relatively long streamwise distance of the shallow water layer to cover relevant wake region. A software was used to evaluate and remove inappropriate displacement vectors (less than 1%), caused by shadows, reflections, or laser sheet distortions in the flow field and replaced by using bilinear interpolation between surrounding vectors in the post-processing step. The field is then smoothed by a Gaussian weighted averaging technique. To minimize distortion of the velocity field, a smoothing parameter of 1.3 is chosen. After constituting vector field, the vorticity patterns of the wake flow were determined by using a finite difference scheme. During each continuous run, a total of 136 images were taken. The time-averaged patterns of the flow structure were calculated by means of these total numbers of instantaneous images. Proper interpretation of the free-surface distortion occurring adjacent to the wake of the cylinder requires accurate determination of the surface coordinates. The coordinates of the surface were tracked using a cursor technique applied to sections of the raw digital tif format image, which was magnified by a factor of approximately 30:1. This technique generates the coordinates of the free surface with an estimated uncertainty of ±0.02 [mm] in the physical plane of the laser sheet.

Adrian [24] and Westerweel [25] provided very detailed information about particle image velocimetry. The uncertainty factors for velocity measurement and vorticity calculation in the PIV method mainly comprised of the seeding particle size, non-uniform particle distribution, particle overlap, unmatched particle correlations, out of laser plane motion (bias and random errors), interrogation window size, and electronic and optical imaging noise. The details of the effects of these factors can be found in the studies of Adrian [24], Westerweel [25], Keane and Adrian [26], Fouras and Soria [27] and Ozgoren [27]. They critically assessed factors contributing to uncertainty in the velocity measurement using the PIV technique and Westerweel [25] calculated the uncertainty in the velocity field as less than 2%.

3. Results and Discussion

3.1. Overview of Patterns of Streamlines and Vorticity

Figure 3 shows the effect of different values of dimensionless cylinder diameter D/h_w = 0.75, 0.5 and 0.25 on the time-averaged streamline patterns and vorticity. Prior to starting each experiment, the cylinder was submerged in the shallow water layer such that its upper surface was coincident with the free-surface. When a steady-state flow was attained, the free-surface tended to glide over the upper surface of the cylinder and form a jet-like flow in the near-wake region. Details of this phenomenon are dependent upon the Froude number. In order to determine the basic classes of flow structure in the near-wake for each cylinder, experiments were carried out at a sufficiently low value of Froude number such that distortions of the free surface were negligible over nearly the entire range of interest. Thin film of water flow over the top of the cylinder and in a region extremely close to the cylinder surface in the near-wake region could not be visualized due to reflection and blockage issues associated with the laser illumination. The possible existence and orientation of this jet-like flow in the wake region could be characterized immediately downstream of the shadow regions (indicated by white background) in each of the images of fig. 3. It is evident from the flow fields located close to each of the cylinders that the streamline topology in the very near-wake of each cylinder is a function of the cylinder diameter and the Froude number associated with the dimensionless cylinder diameters D/h_w.

Viewing each of the flow fields of fig. 3. as a whole; it is evident that well-defined reattachment of location is a common feature which is indicated by the vertical arrow immediately adjacent to the free-surface. For D/h_w = 0.75 configuration, a circulating bubble or developing focus which are designated as F_1 is formed. A primary circulating bubble which is designated as F covers most part of the wake flow region just downstream of the developing focus F_1. Between developing and primary focus a saddle point designated as S took place. In the case of D/h_w = 0.50, an unstable focus F_2 that is the streamlines spiral outward starting from the central point of the focus is developed close to downstream of the cylinder surface, developing and primary foci F_1, F covered the rest of the wake flow region. Between the foci F_1 and F_2, a saddle point S is evident. For the case of D/h_w = 0.25, the wake region with foci F_1 and F_2 are identifiable and then the saddle point S is formed just beneath the free-surface. Furthermore, each of these developing and primary cells has a stable focus that is the streamlines spiral towards inward the central points of foci.

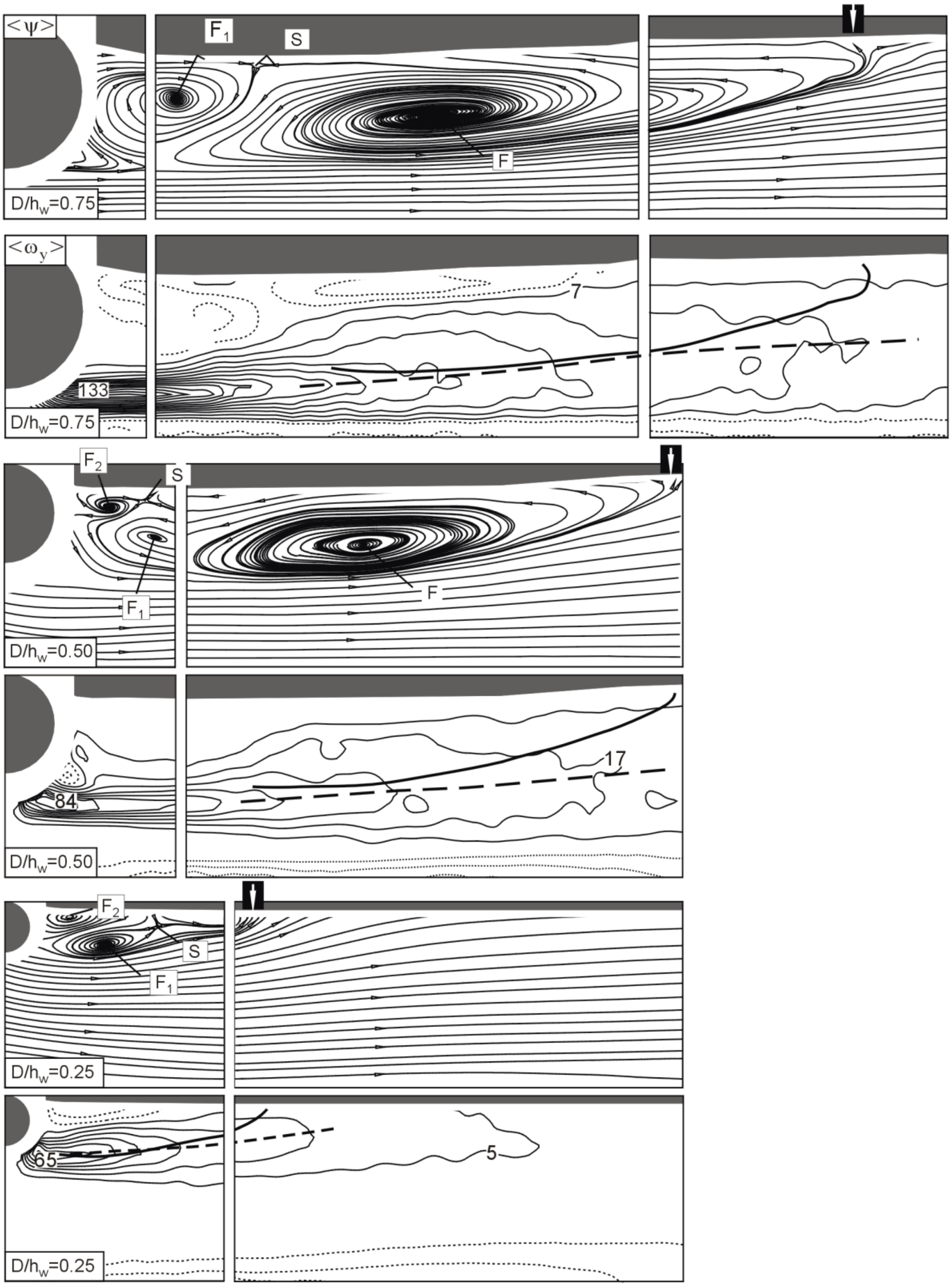

Figure 3. Overviews of time-averaged of streamlines <*ψ*> and vorticity <*ω*> patterns for *D/h*$_w$=0.75 , 0.50 and 0.25. For all images, the minimum and incremental values of vorticity are $\omega_{min}=\pm 8\ s^{-1}$ and $\Delta\omega= 8\ s^{-1}$

The shear layer formed from the lower surface of the cylinder has a magnitude of time-averaged vorticity $<\omega_y>$ that rapidly decreases when the dimensionless values of D/h_w decrease. Peak values of time-averaged vorticity are found to be 133, 84 [s^{-1}] and 65 [s^{-1}] associated with D/h_w = 0.75, 0.5 and 0.25 respectively as seen in fig. 3. For each of these patterns of the time-averaged vorticity $<\omega_y>$, the line which is designated with dash line corresponds to the approximate center of each of the contours of constant vorticity $<\omega_y>$. On the other hand, the solid-line corresponds to the streamline which reattaches to the free surface first. It is clear that these two lines are coincident in the upstream region, but they rapidly diverge in the downstream region as the flow approaches to reattachment location. The length of the wake flow region in the streamwise direction is varied as a function of D/h_w. A high rate of jet-like flow exists between bed surface and lower surface of the cylinder for D/h_w=0.75. As seen from the time-averaged streamline patterns in fig. 3., the reattachment distances from the base of the cylinder were determined as 3.65xh_w, 3.02xh_w and 1.13xh_w for D/h_w = 0.75, 0.5 and 0.25, respectively.

3.2. Comparison of Reynolds Stress Correlations, Time-averaged Velocity, Streamline and Vorticity Patterns

Figures 4a and 4b present the time-averaged velocity vector $<V>$, corresponding patterns of streamline $<\psi>$, vorticity $<\omega>$ and Reynolds stress correlations $<u'v'>/U^2$ The flow fields of views were chosen in order to include the regions of high Reynolds stress correlations and the location of core flow reattachment to the free-surface. For this reason, in the largest cylinder case as D/h_w = 0.75, it was necessary to employ two flow fields of view, as indicated in fig. 4a. Furthermore, on each pattern of Reynolds stress correlations, the thick bold black line indicates the boundary of wake regions with the core flow and the locus of the reattachment streamline to the free-surface.

As shown in fig. 4a., the peak values of Reynolds stress correlations $<u'v'>/U^2$ generally followed the reattachment streamline or along the shear layer where a high rate of interactions and circulatory flow motions occur between the core and wake flow regions. In turn, the locus of this reattachment streamline is generally in accord with the peak values of averaged vorticity $<\omega>$ and regions of large gradients of time-averaged velocity $<V>$. As the location of reattachment is approached, however, the major effects occur. First of all, the magnitude of the maximum value of Reynolds stress correlations $<u'v'>/U^2$ decreases from its peak value to a moderate level at a location further downstream. Secondly, as the reattachment point itself is approached, the locus of the streamline reverses in the upstream direction cutting the last line of contours which presents the lowest value of constant Reynolds stress correlations $<u'v'>/U^2$ occurring in the close proximity of the free surface. The magnitude of Reynolds stress correlation $<u'v'>/U^2$ keeps its strength until the reattachment point due to a high rate entrainment between wake and core flow regions and then it decays down while the vortical flow travels in the downstream direction. This feature is consistent for all values of dimensionless cylinder diameter D/h_w. This observation suggests that the instantaneous physics of the flow associated with high values of Reynolds stress correlations $<u'v'>/U^2$ at the upper region of the reattachment location persists further downstream in the flow direction for a longer distance comparing to the time-averaged flow data. As described in the next section, well-defined clusters of vortical structures that are generated in the shear layer of upstream of the reattachment locations move further downstream in the flow direction due to the increase in momentum transfer. In addition to flow physics explained for fig. 4a., the wake region reattaches to the free surface in a shorter distance when the dimensionless cylinder diameters were taken as D/h_w = 0.50 and D/h_w = 0.25 shown in fig. 4b. An effected area of flow region and the magnitude of the velocity vectors <V>, streamline patterns $<\psi>$, vorticity contours $<\omega_y>$ and Reynolds stress correlations $<u'v'>/U^2$ attenuate due to the lowering the dimensionless cylinder diameters D/h_w.

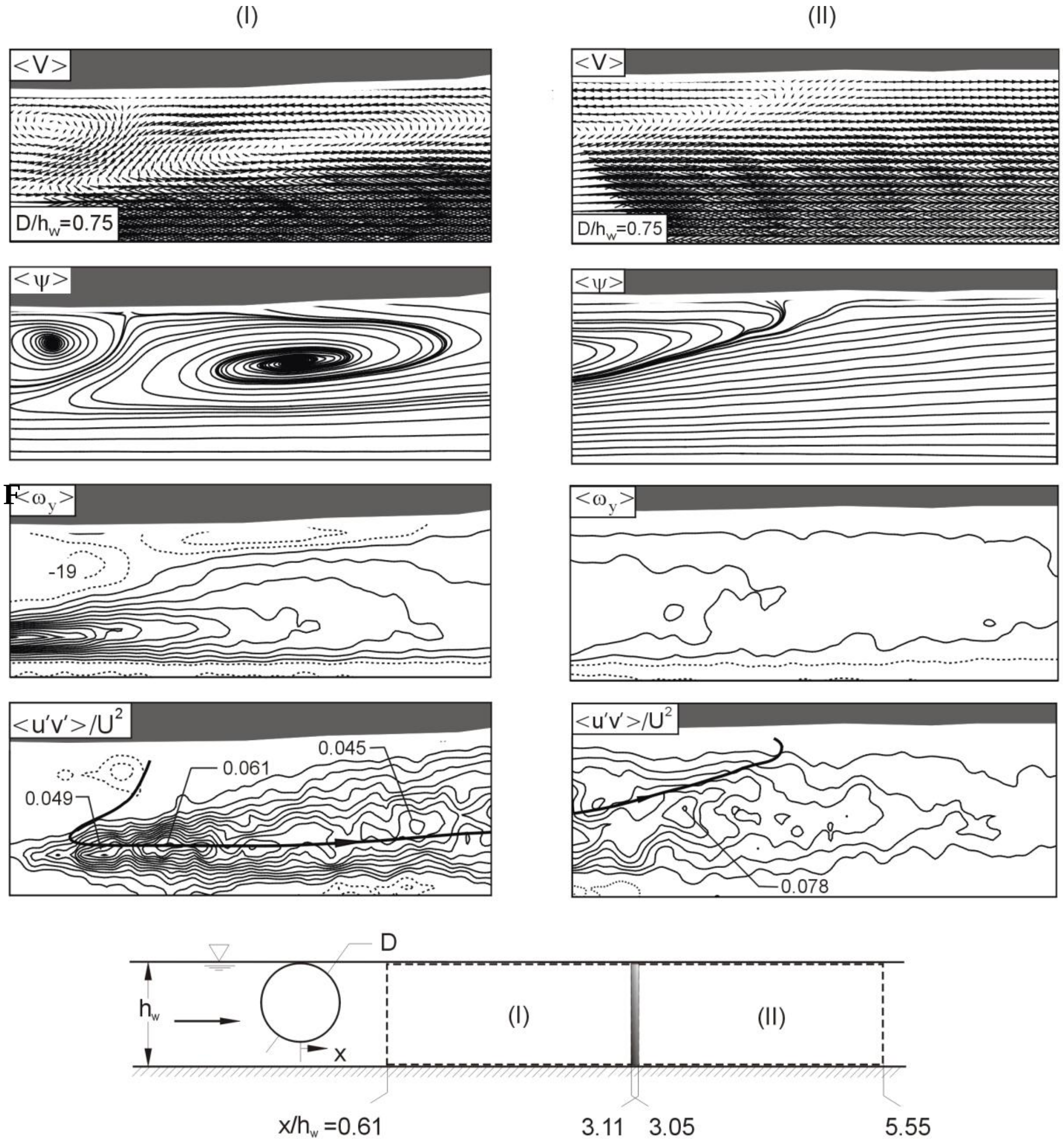

Figure 4a. Time-averaged streamlines <ψ>, velocity vectors, vorticity <ω_y> patterns and normalized Reynolds stress <$u'v'$>/U^2 downstream of a horizontal cylinder for D/h_w=0.75. Sketch shows the location of laser sheet. For all images, minimum and incremental values of vorticity and normalized Reynolds stress are ω_{min}=± 8 s^{-1} and Δω=8 s-1, [<$u'v'$>/U^2]$_{min}$=± 0.005 and Δ[<$u'v'$>/U^2]=0.005 respectively.

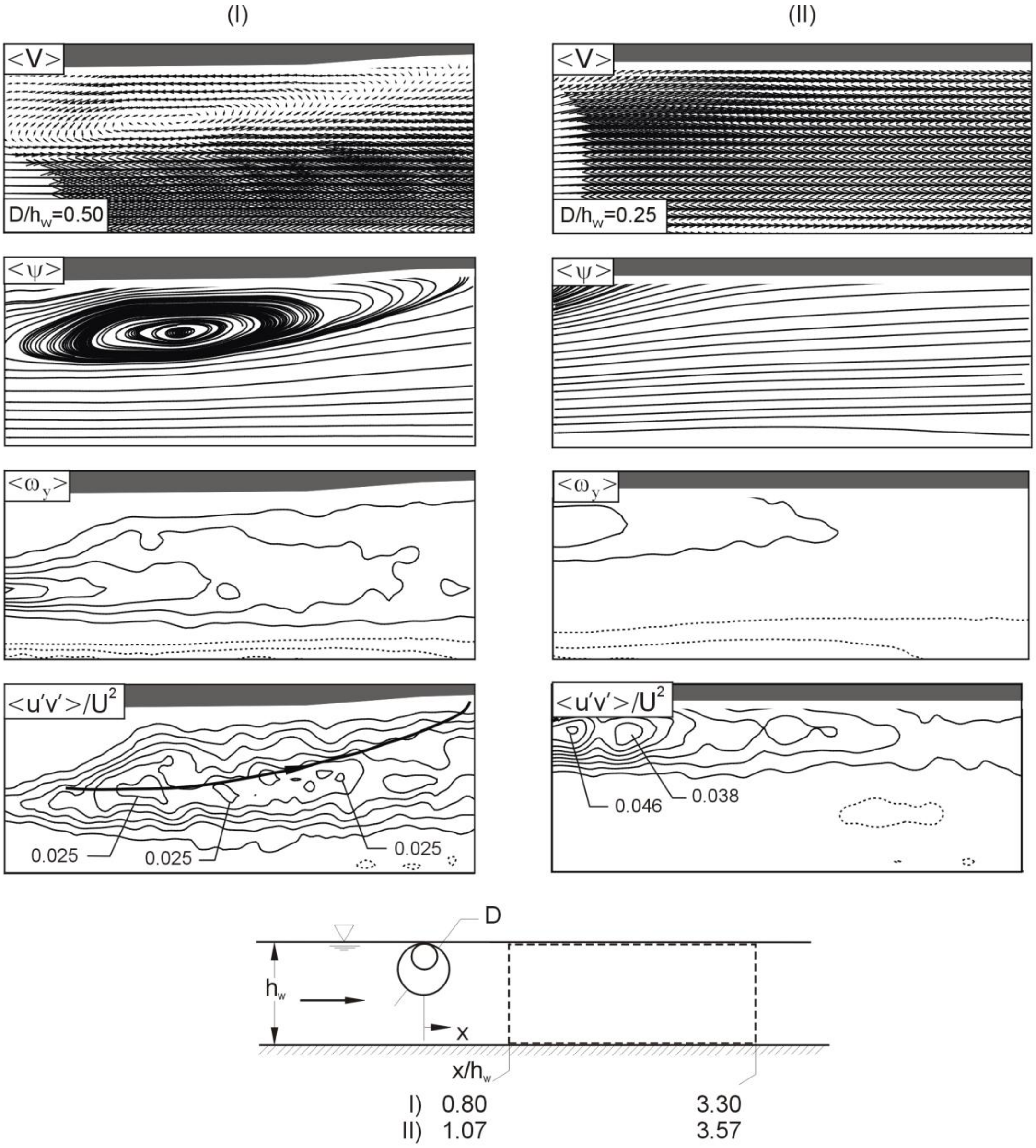

Figure 4b. Time-averaged streamlines <ψ>, velocity vectors, vorticity <ω_y> patterns and normalized Reynolds stress <*u'v'*>/U^2 downstream of a horizontal cylinders for D/h_w=0.25, 0.50. Sketch shows the location of laser sheet. For all images, minimum and incremental values of vorticity and normalized Reynolds stress are $\omega_{min}=\pm$ 8 s^{-1} and $\Delta\omega$=8 s^{-1}, [<*u'v'*>/U^2]$_{min}=\pm$ 0.005 and Δ[<*u'v'*>/U^2]=0.005 respectively.

3.3. Instantaneous Velocity and Vorticity Patterns

Figure 5 presents randomly selected representative instantaneous patterns of vorticity and velocity vectors for cases of D/h_w = 0.75, 0.5 and 0.25. A length of open gap between bed and lower surface of the cylinder is one fourth of the water level for the case of D/h_w = 0.75. So, jet-like flow is evident through this open gap as seen in the first and second rows of fig. 5. A concentrated vortex cluster expands along the shear layer in the downstream direction. A substantial reduction takes place in the level of the vorticity due to the expansion of core-flow region in streamwise direction. For the cases of D/h_w =0.5 and 0.25, instantaneous patterns of vortices and velocity vectors indicate that core flow regions expand in size in the streamwise direction while the main flow travels further downstream. The length of reattachment of core flow with the free surface is shorter than the case of D/h_w = 0.75. The location of reattachment point is not clearly defined by the instantaneous velocity vectors V, because the point of the reattachment moves forward and backward randomly. Through the observation of an animation of instantaneous images, it is seen that small-scale concentrations of vorticity convey the fresh fluid into the wake flow region magnifying the entrainment between the core flow and wake flow regions. Due to this reason, the size of the wake flow region with the lowest entrainment is the smallest in the case of D/h_w =0.25. This flow phenomenon happens because of the larger gap between the bed surface and the lower surface of the cylinder. Instantaneous locations of reattachment points move backward and forward in the direction of the free stream flow due to the instability of the vortical flow structure. The central line of shear layer also move in upper and lower direction for the same reason. Flow patterns of vorticity show distinctive small-scale concentrations embedded in the larger-scale structures. They induce new types of elongated large-scale structures in the near-wake region, thus extending recirculation bubble. In fact, these identifiable structures of vorticity exist even at region well downstream of the reattachment point. It is therefore evident that the origin of the regions of high Reynolds stress correlations $<u'v'>/U^2$ shown in fig. 4a. and fig. 4b., are coincidence with these well-defined small-scale concentrations of vorticity and their conglomeration.

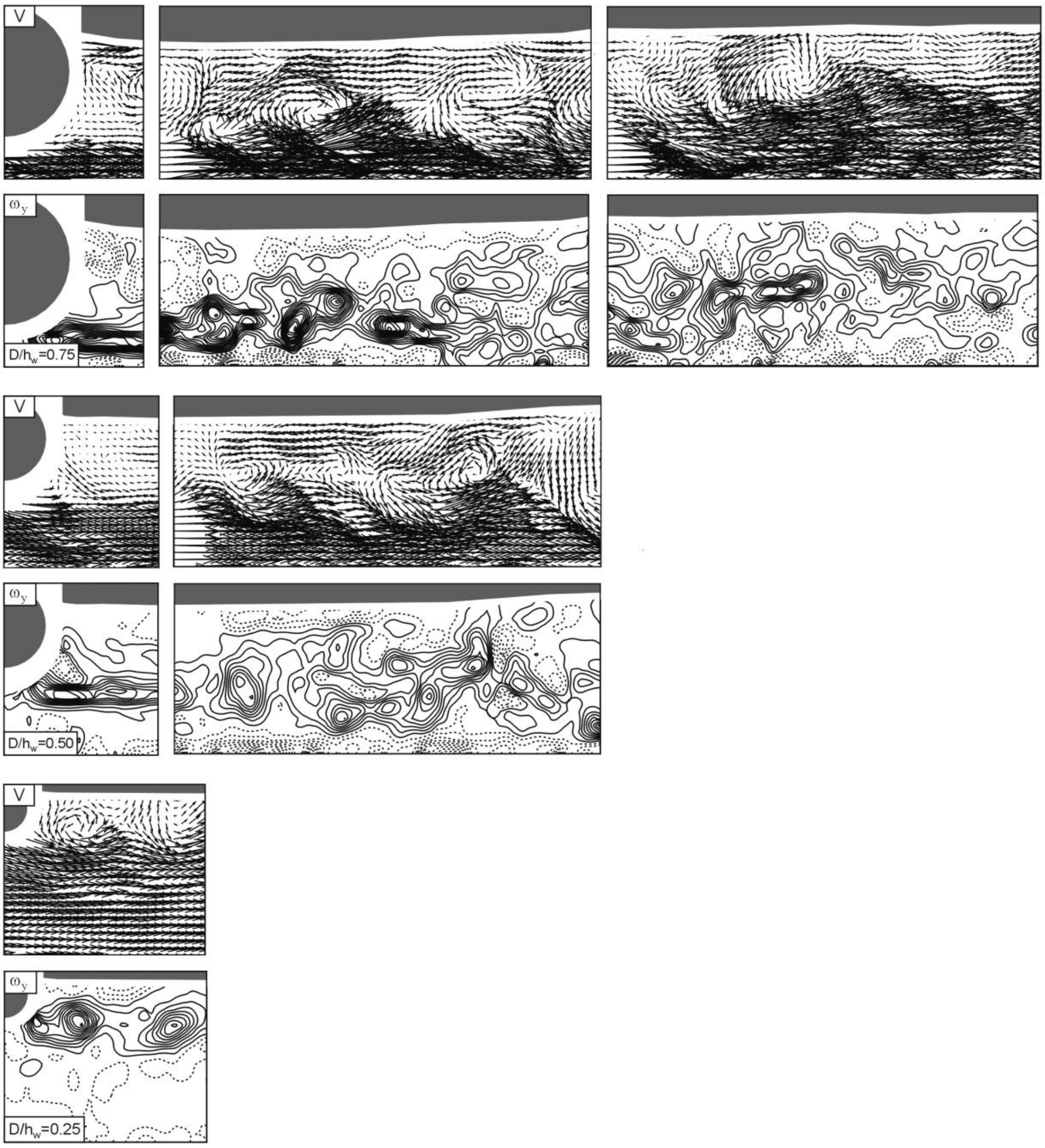

Figure 5. Instantaneous velocity vectors V and vorticity patterns ω_y in the near-wake region of a horizontal cylinder for D/h_w=0.75, 0.5, 0.25. For all images, minimum and incremental values of vorticity are $\omega_{min}=\pm$ 8 s^{-1} and $\Delta\omega$=8 s^{-1}

3.4. Three-Dimensional Flow Structure

Figure 6a gives an overview of patterns of instantaneous velocity; streamline patterns and corresponding vorticity at various cross-sectional cuts A through D, which extend from the region of the separated shear layer immediately downstream of the cylinder to a location near the flow reattachment. At all cross-sectional locations, the patterns of velocity vectors show regions of localized swirl. They are associated with well-defined concentrations of streamwise vorticity (ω_x).

At location AA, the pattern of streamwise vorticity is centered at an elevation from the bottom surface corresponding approximately to the locus of maximum spanwise vorticity ω_y. In other words, these structures clearly arise in the separated shear layer from the cylinder. Spanwise spaces between positive and negative vorticity centers depending on the cross sections at location AA vary in the range from 0.62xD to 0.2xD. The peak value of vorticity of the streamwise concentration ω_x is 68.3 [s^{-1}]. This value is lower than the peak levels of vorticity ω_y values ranging from 162.5 [s^{-1}] to 199.2 [s^{-1}]presented in the instantaneous flow data images in fig. 5. At locations further downstream, along the recirculation zone and in the vicinity of reattachment, i.e., sections BB through DD, the concentrations of vorticity ω_x occupy regions successively closer to the free-surface until section DD. Pronounced concentrations of streamwise vorticity of alternating sign occur immediately beneath the free-surface. The average spanwise spacing in these concentrations at section DD is of the order of 0.40 D. Furthermore, the peak values of vorticity over the entire section DD are in the range of 50.1 [s^{-1}]to 26.5 [s^{-1}]. It is therefore concluded that the scale of the streamwise vorticity concentrations ω_x is relatively unaffected by the cross-sectional location along the reattachment zone. Furthermore, the peak values of vorticity ω_x show only a mild decrease in the region of the shear layer immediately downstream of separated flow region, i.e. at DD.

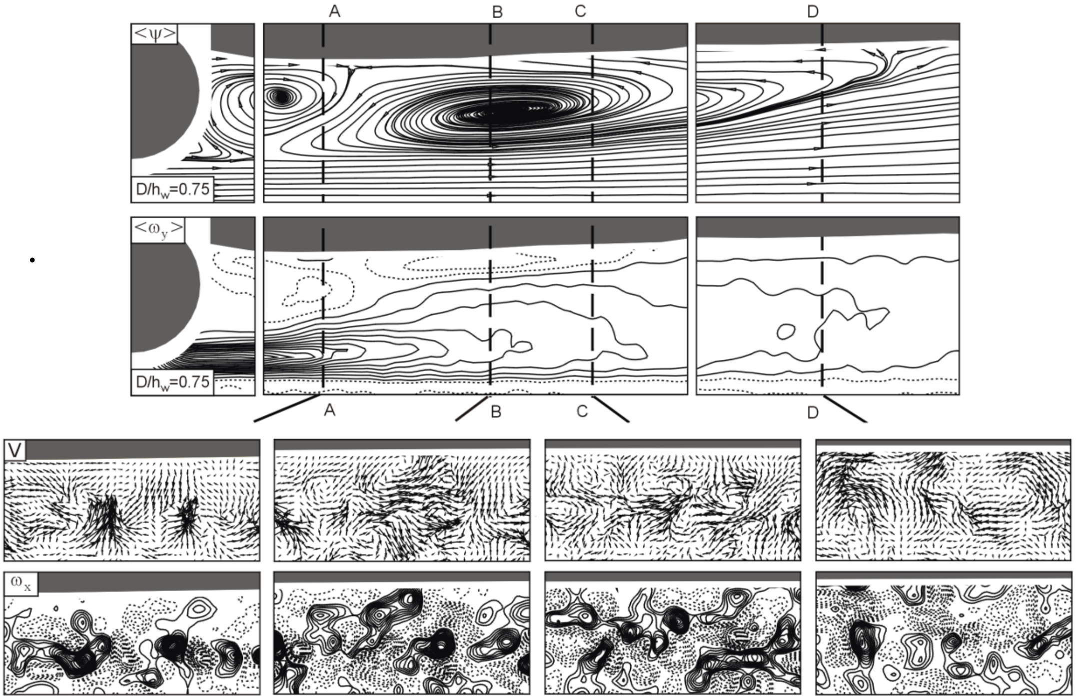

Figure 6a. Overview of patterns of instantaneous velocity *V* and streamwise vorticity ω_x at various cross-sectional cuts A through D, which extend from the region of the separated shear layer immediately downstream of the horizontal cylinder to a location near flow reattachment for D/h_w=0.75. For all images, minimum and incremental values of vorticity are $\omega_{min}=\pm 4\ s^{-1}$ and $\Delta\omega=4\ s^{-1}$

Further features of the three-dimensionality at cross-sections AA and DD are shown in fig. 6b., in the form of time-averaged streamline and velocity vectors patterns over the respective cross-sections. At location AA, the predominant features are relatively large velocity vectors in the downward direction, due to the entrained flow demanded by the developing shear layer from the surface of the cylinder. The corresponding pattern of streamlines shows a series of convergent nodal lines denoted L_c at an elevation corresponding to the edge of the vorticity layer ω_y that separates from the surface of the cylinder. This convergent nodal line involves spatially periodic occurrence of saddle points S_a and S_b. Furthermore, at the free-surface, the streamlines tend to merge into local nodes of the form indicated by N_b. At location DD, however, such convergent nodal lines L_c, nodes N_b and saddle points S no longer occur. The flow is generally directed towards the free-surface, due to the process of reattachment indicated by the quasi-two-dimensional streamline patterns in the top set of images. Occurrence of foci F_a and F_b represent the three-dimensionality at this section.

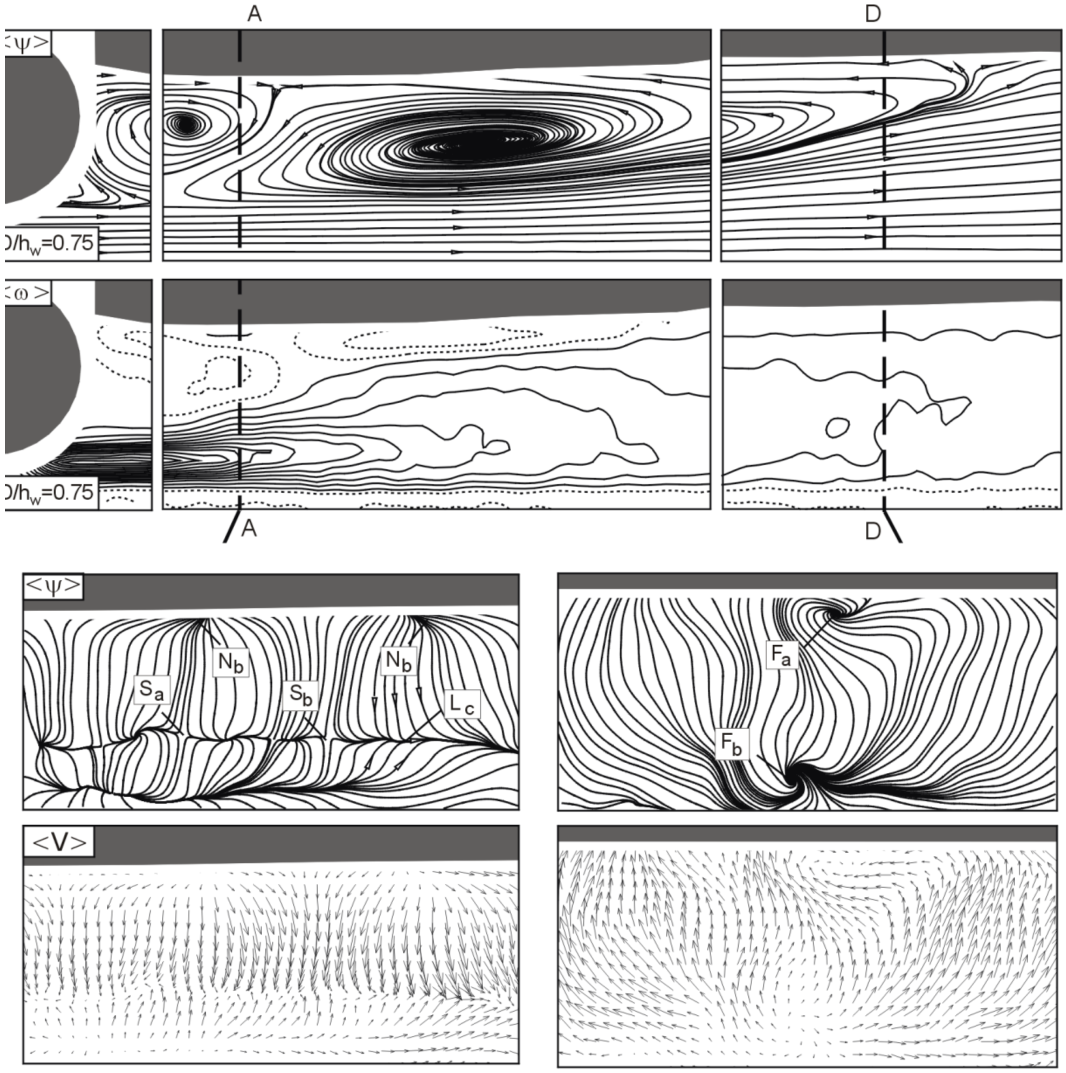

Figure 6b. Overview of patterns of time-averaged velocity <*V*> and streamlines <*ψ*> at cross-sectional A and D, which extend from the region of the separated shear layer immediately downstream of the horizontal cylinder to a location near flow reattachment for D/h_w=0.75.

4. Conclusions

The physics of near-field vortex development for the horizontal cylinder in shallow water has been represented by global patterns of velocity, vorticity and streamline pattern. This approach has allowed observing the surface (bed) flow patterns in relation to the flow away from the surface, and provide a basis for understanding the bed loading associated with the initial stages of erosion and transportation of sediment.

The diameter of cylinder was varied with small increments in order to determine the effect of open gap between the bed surface and the cylinder surface and major changes in the near-wake flow patterns. For the cases of dimensionless cylinder diameters such as D/h_w = 0.75, 0.5 and 0.25, variation of the streamline patterns in very near-wake of each cylinder substantially depends on the dimensionless the cylinder diameter D/h_w and the Froude number, presently taken as $Fr=U/(gD)^{1/2}$ =0.41, 0.50 and 0.71 associated with the value of D/h_w = 0.75, 0.5 and 0.25, respectively. The counter-flow in the upstream direction along the mixing layer exists where developing recirculation cell with a focus F_1 occurs. On the other hand, the primary recirculation bubble as indicated by streamline patterns in fig. 3. shows that the direction of rotation opposes the direction of developing recirculation cell. However, occurrence of entrainment between free-surface and the mixing layer induces the flow transfer between core and wake flow regions. Counter-flow rotation in the upstream direction occurs for cases of D/h_w = 0.75 and D/h_w = 0.50. The circulating bubbles F and F_1 rotate in clockwise while F_2 rotates in anti-clockwise. It can be concluded that the rate of entrainment is higher when the counter-flow direction opposes the direction of core flow along the mixing layer as seen in the case of D/h_w = 0.75. A high rate of entrainment may increase the unsteadiness of the flow. The magnitude of jet velocity increases by increasing the diameter of the cylinder causing concentrated positive vorticity. The mixing layer in the downstream region of the flow is dominated by the positive vorticity as seen in fig. 3. For the case of D/h_w = 0.75, a jet-like flow, which glides over the top surface of the cylinder, is evident immediately beneath the free-surface. This surface jet-like flow stimulates the developing recirculation bubble which rotates in clockwise as indicated by streamline patterns and vector velocity.

The Reynolds stress correlations $<u'v'>/U^2$ values are the greatest at a location around the maximum vorticity concentration region. A high level of Reynolds stress fluctuations exists along the shear layer. Entrainment process may be the cause of the high rate of Reynolds stress fluctuations. Instantaneous physics of flow that is associated with high values of Reynolds stress correlations $<u'v'>/U^2$ along the shear layer persists further downstream of the reattachment point. After a certain distance, the magnitude of Reynolds stress correlations $<u'v'>/U^2$ diminishes as the core flow reconstructs itself to become a fully developed flow. Instantaneous patterns of vorticity indicate that a well-concentrated vorticity occurs along the shear layer. A substantial deterioration in the level of the vorticity happens due to the enlargement of the core flow region while the main flow moves further downstream. Viewing all images together show that concentrated vortices expand gradually and diminish while flow proceeds further downstream in the longitudinal direction depending on the cylinder diameter.

Acknowledgements

The authors would like to thank Professor Donald Rockwell for letting them carry out this experimental study at the Fluid Mechanics Laboratory of Lehigh University, USA, and for his many valuable discussions and suggestions on this topic. The authors thank to the BAP office of Selcuk University.

Nomenclature

D – diameter of cylinder, [mm]
Fr – Froude number based on the water depth ($=U/(gh_w)^{1/2}$, [-]
H – boundary layer shape factor ($=\delta^*/\theta$),[-]
h_w – height of water level [mm]
Re – Reynolds number based on the diameter of cylinder ($= UD/\nu$), [-]
U – free stream velocity (maximum velocity), [mms^{-1}]
$u'v'$ – Reynolds stress correlation, [mm^2s^{-2}]
V – instantaneous velocity, [mms^{-1}]
$<V>$ – time-averaged total velocity vector, [mms^{-1}]
$<\omega>$ – time-averaged vorticity, [s^{-1}]
$<\omega_y>$ – time-averaged spanwise vorticity, [s^{-1}]
ω_x – instantaneous streamwise vorticity, [s^{-1}]

Greek letters

$<\psi>$ – time-averaged streamline,[-]
δ – boundary layer thickness, [mm]
δ^* – displacement thickness of boundary layer, [mm]
θ – momentum thickness of boundary layer, [mm]
ν – kinematic viscosity, [mms^{-2}]

References

[1] Kahraman, A., Sahin, B. and Rockwell, D., Control of vortex formation from a vertical cylinder in shallow water: Effect of localized roughness elements, *Experiments in Fluids, 33* (2002), pp. 54–65

[2] Akilli, H. and Rockwell, D., Vortex formation from a cylinder in shallow water, *Physics of Fluids 14* (2002), 9, pp. 2957-2967

[3] Lin, J. C., Ozgoren, M. and Rockwell, D., Space–time development of the onset of a shallow-water vortex. *Journal Fluid Mechanics, 485* (2003), pp. 33–66

[4] Ingram, R. G. and Chu, V. H., Flow around island in Rupert Bay: an investigation of the bottom friction effect, *Journal of Geophysical Research, 92* (1987), pp. 14521–14533

[5] Chen, D. and Jirka, H., Experimental study of plane turbulent wakes in a shallow water layer, *Fluid Dynamics Research, 16* (1995), pp. 11–41

[6] Akilli, H., Akar, A. and Karakus, C., Flow characteristics of circular cylinders arranged side-by-side in shallow water, *Flow Measurement Instrumentation*, *15* (2004), pp. 87–197

[7] Triantafyllou, G. S. and Dimas A. A., The low Froude number wake of floating bluff objects, Internal Report MITSG89-5, Massachusetts Institute of Technology, Cambridge, Massachusetts, USA, 1989a

[8] Triantafyllou G. S. and Dimas A. A. Interaction of two-dimensional separated flows with a free surface at low Froude numbers. *Physics of Fluids* A 1 (1989b), pp. 1813–1821

[9] Yu, D. and Tryggvason, G., The free surface signature of unsteady two dimensional vortex flows. *Journal of Fluid Mechanics, 218* **(**1990), pp. 547–572

[10] Tryggvason, G., Unverdi, S. O., Song M. and Abdolahi-Alibeik J., Interaction of vortices with a free surface and density interfaces, in: *Vortex Dynamics and Vortex Methods, In Lectures in Applied Mathematics* (Ed. C. R. Anderson and C. Greengard), American Mathematical Society, 28, 1991, pp. 679–699

[11] Rood, E. P., Vorticity interactions with a free surface, in: *Fluid Vortices*, (Ed. S. I. Green), Kluwer Inc., 1995, pp. 687–730

[12] Sheridan, J., Lin, J. C. and Rockwell, D., Metastable states of a cylinder wake adjacent to a free surface, *Physics of Fluids, 7* (1995), pp. 2099–2101

[13] Sheridan, J., Lin, J. C. and Rockwell, D., Flow past a cylinder close to a free surface. *Journal of Fluid Mechanics,* 330 (1997), pp. 1–30

[14] Hoyt, J. W. and Sellin, R. H. J., A comparison of the tracer and PIV results in visualizing water flow around a cylinder close to the free surface, *Experiments in Fluids, 28* (2000), pp. 261–265

[15] Bearman, P. W. and Zdravkovich, M. M., Flow around a circular cylinder near a plane boundary. *Journal of Fluid Mechanics, 89* (1978), pp. 33-47.

[16] Reichl, P. J., Hourigan, K. and Thompson, M. C., The unsteady wake of a circular cylinder near a free surface, *Flow, Turbulence and Combustion, 71* (2003), pp. 347–359.

[17] Reichl, P. J., Hourigan, K. and Thompson, M. C., Flow past a cylinder close to a free surface, *Journal of Fluid Mechanics, 533* (2005), pp. 269–296.

[18] Ozturk, N. A., Akkoca, A. and Sahin, B., Flow details of a circular cylinder mounted on a flat plate, *Journal of Hydraulic Research, 46 (*2008), 3, pp. 334-355.

[19] Sahin, B. and Ozturk, N. A., Behaviour of flow at the junction of cylinder and base plate in deep water, *Measurement, 42* (2009), pp. 225–240.

[20] Kirkgöz, M. S. and Ardiçlioğlu, M. Velocity profiles of developing and developed open channel flow, *Journal of Hydraulic Engineering, 123* (1997), pp. 1099-1105.

[21] Klenanoff, P. S., Characteristics of turbulence in a boundary layer with zero pressure gradient, NACA Technical Notes, No. 1347, Washington, D. C, USA, 1955

[22] Purtell, L. P., Klebanoff, P. S. and Buckley, F. T., Turbulent boundary layer at low Reynolds numbers, *Physics of Fluid, 24* (1981), pp. 802-811.

[23] Johansen, J. B. and Smith, C. R., The effects of cylindrical surface modification on turbulent boundary layers, Report FM-3, Department of Mechanical Engineering and Mechanics, Lehigh University, Bethlehem, PA, USA, 1983.

[24] Adrian, R. J., Particle-imaging techniques for experimental fluid mechanics, *Annual Review of Fluid Mechanics*, *23* (1991), pp. 261–304.

[25] Westerweel, J., Digital particle image velocimetry, theory and application, Delft University Press, Netherlands, 1993.

[26] Keane, R. D. and Adrian, R. J., Optimization of particle image velocimeters, *Optical Methods in Flow and Particle Diagnostics, 68* (1989), pp. 139–59.

[27] Fouras, A. and Soria, J., Accuracy of out-of-plane vorticity measurements derived from in-plane velocity field data, *Experiments in Fluids, 25* (1998), pp. 409–430.

[28] Ozgoren, M., Flow structure in the downstream of square and circular cylinders, *Flow Measurement Instrumentation, 17* (2006), pp. 225–235.